Sensitivity of global network dynamics to local parameters versus motif structure in a cortexlike neuronal model

E. Kopelowitz,[1,2] M. Abeles,[2] D. Cohen,[2] and I. Kanter[1,2]

[1]*Minerva Center and Department of Physics, Bar-Ilan University, 52900 Ramat-Gan, Israel*

[2]*Gonda Interdisciplinary Brain Research Center and the Goodman Faculty of Life Sciences, Bar Ilan University, Ramat-Gan 52900, Israel*

(Received 23 May 2011; revised manuscript received 4 January 2012; published 1 May 2012)

In the field of network dynamics it has been suggested that statistical information of motifs, small subnetworks, can help in understanding global activity of the entire network. We present a counterexample where the relation between the stable synchronized activity modes and network connectivity was studied using the Hodgkin-Huxley brain dynamics model. Simulations indicate that small motifs of three nodes exhibit different synchronization modes depending on their local parameters such as delays, synaptic strength, and external drives. Thus the activity of a complex network composed of interconnected motifs cannot be extracted from the activity mode of each individual motif and is governed by local parameters. Finally, we exemplify how local dynamics ultimately enriches the ability of a network to generate diverse modes with a given motif structure.

DOI: 10.1103/PhysRevE.85.051902 PACS number(s): 87.85.dm, 87.19.lj, 87.18.Sn, 05.45.Xt

I. INTRODUCTION

In recent years, the vast network dynamics literature has increasingly focused on finding classification measures that will be suitable for large networks of different disciplines such as the worldwide web links, neural networks, social networks, etc. [1–6]. Milo *et al*. [5,6] classified networks according to topological motifs (small subgraphs) that appear significantly more often than in random networks. They found that similar motifs appear in networks that perform information processing such as neural networks and suggested that the similarity in their statistics indicates that they play an important role in the global functionality of a network.

There have been some attempts to relate topological structure of neural networks to their functionality [7,8]. EEG records on multiple brain areas as well as theoretical models have reported correlations and synchronization between two or more cortical areas for periodic activity both in the high-frequency range (around 50 Hz gamma activity), and for very slow waves (delta activity) [9]. Near zero-lag synchronization (ZLS) was suggested as a marker of binding activities in different cortical visual areas into one perceptual entity [10,11], leading to the hypothesis that the emergence of synchronization in neural networks may hold information about the functionality of the network.

Combining these two conjectures, one might ask what is the relation between the motif structure of a network and the synchronization state? Consider a network with one motif. Does topology alone determine its dynamical activity, or do the network parameters of the motif control its behavior? We define the topology of a network as the connectivity between nodes, and the network parameters as the specifics of the connections such as strengths and length that indicates transmission time delays. If the interplay between the network parameters of a motif and its behavior is known, two possible scenarios for the dynamic behavior of a network composed of several interconnected motifs are possible. The first is that every motif maintains its behavior, and the entire behavior of a network is simply described as interconnected building blocks of connecting components with given activity modes; hence their statistics are of interest. The second scenario is that the activity mode of the entire network is governed by nonlocal behavior inducing long-range effects. In this case, changing some specific parameters at the end of the network, for example, will affect the dynamics and the synchronization properties of the rest of the network. Note that each neuron is governed by a nonlinear function [12] where small perturbations in its specific parameters may cause dramatic changes in the dynamics and can lead to various bifurcations (changes from stationary to periodic to chaotic behavior) [13]. In this study, however, we focus on the periodic regime of the neuron dynamics [14,15] and investigate the relation between the networks parameters (i.e., connection length, etc.) and the global dynamical prosperities of the network.

We demonstrate that in the case of neural networks, the knowledge of motif statistics is not sufficient in order to describe the behavior of the entire network. We study the stable synchronized activity modes of neural networks whose connectivity mimic the intercolumnar connectivity of the neocortex using the Hodgkin-Huxley model for the single neuron [16]. We first show that a motif exhibits several different firing patterns and synchronization states depending on its parameters. We posit that biological activities are determined by comprehensive motifs characterized by both the topology and network parameters of individual motifs. When several motifs are interconnected to a network, they typically do not maintain their local activity and a combined global activity takes over the dynamics of the entire network. This global activity is governed by long-range correlations resulting in sensitivity to local changes in parameters of the network, such as connectivity, synaptic strengths, and delay times.

II. THE MODEL

A neural network consists of nerve cells (neurons) linked to each other by synapses. A typical neuron possesses a cell body—the soma, dendrites, and an axon. Dendrites are filaments that arise from the cell body and branch multiple times, giving rise to a complex dendritic tree. An axon is a special cellular filament that arises from the soma and travels for a distance. All neurons are electrically excitable,

maintaining voltage gradients across their membranes. If the voltage gradients are increased by a large enough amount, an all-or-none electrochemical pulse called an action potential (AP) is generated, and travels rapidly along the cell's axon and finally activates synaptic connections with other neurons. The effect upon the target neuron can be excitatory (increasing the voltage gradient) or inhibitory (decreasing the voltage gradient) [12].

To explore the local and nonlocal behavior of cortical neural activity, a realistic numerical model was designed in which the dynamic behavior of a solitary neuron, delays, background noise, and connectivity strength were taken into account. Every neural cell was simulated using the well-known Hodgkin-Huxley (HH) model [16] and in terms of biological properties it was assumed that distant cortico-cortical connections are (almost) exclusively excitatory whereas local connections are both excitatory and inhibitory [12,17].

In our network model, each node represents one cortical patch comprised of a population of N HH neurons. The mean firing rates of the cortex in an awake state are low and irregular [18], whereas the firing rates of the HH model subject to constant excitatory current are periodic and very high, typically around 80 Hz. Low and irregular firing rates were achieved in our model by introducing a balance between excitatory and inhibitory neurons. Specifically the population was selected to be 80 (20) percent of excitatory (inhibitory) neurons [12,19,20] [demonstrated for two nodes in Fig. 1(a) (left)]. For simplicity, connections between pairs of excitatory

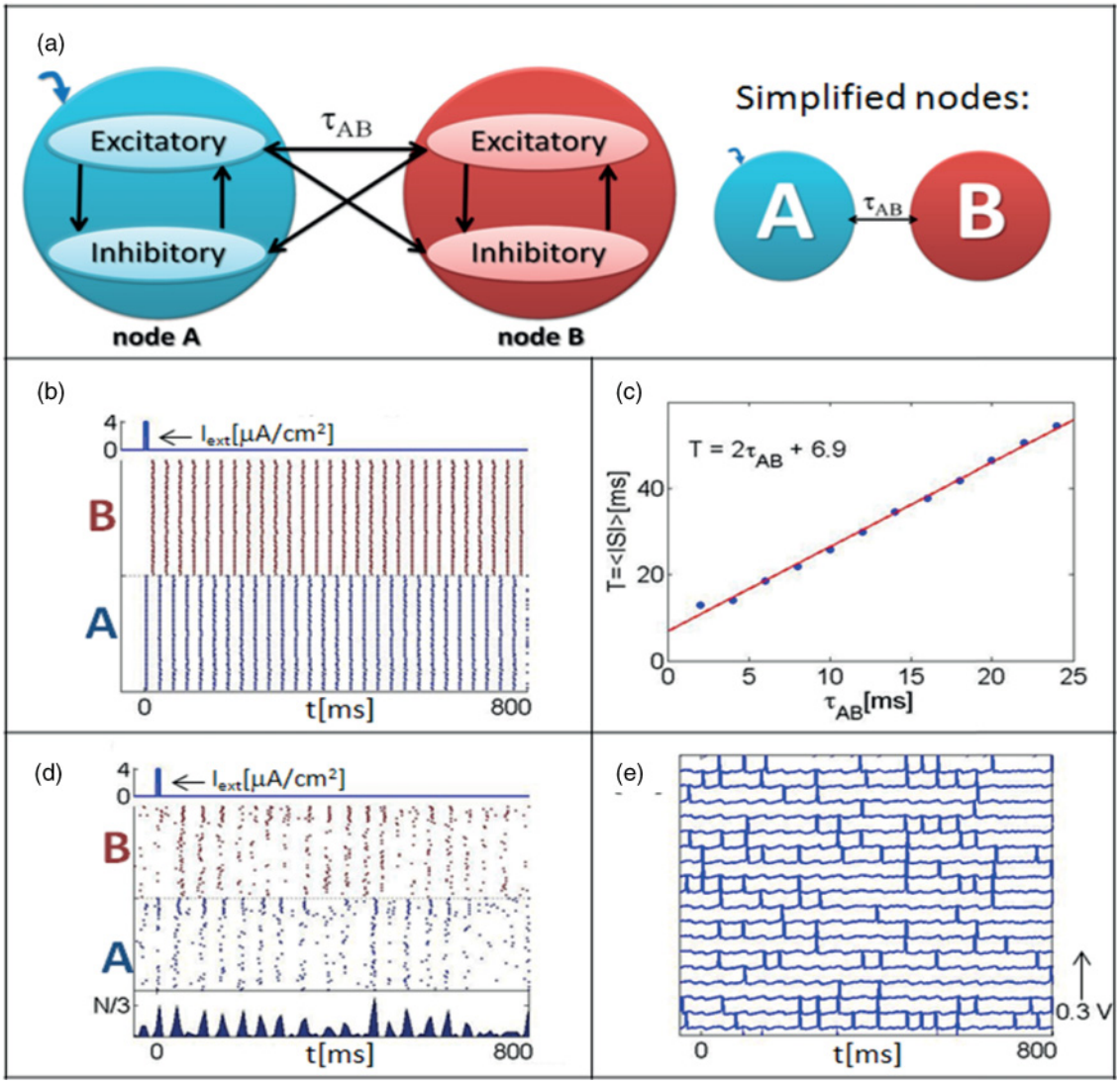

FIG. 1. (Color online) (a) Left: Schematic diagram of two mutually connected nodes representing populations of neurons. Each node comprises excitatory and inhibitory neurons. The connections are sparse, pairs of neurons belonging to the same node are connected with probability $p_{\text{in}} = 0.8$ and pairs of neurons belonging to two nodes are connected with probability, $p_{\text{out}} = 0.2$. The small blue arrow on top of the left corner of node A represents a short stimulus. Right: Schematic diagram of two connected simplified nodes. Each node comprises excitatory neurons, other properties remain the same. (b) Raster diagram of the firing activity of two connected simplified nodes (with no background noise and no inhibitory connections). (c) Average ISI as a function of the average delay, τ_{AB}, between the two populations. (d) Raster diagram of the same network with background noise and inhibitory connections. Bottom panel: histogram of spike timings of neurons in node A. (e) Spike trains of several neurons from node A. Simulations parameters are: $N = 60$, synaptic strength $g_{\max} = 0.72\ \text{mS/cm}^2$, $I_{\text{ext}} = 4\ \mu\text{A/cm}^2$, $\tau_{AB} = 10$ ms.

and inhibitory neurons were selected with probability $p_{\text{in}} = 0.8$, however, results remain robust with additional excitatory-excitatory and inhibitory-inhibitory connections. A connection between neurons belonging to different nodes was excitatory only and was selected with probability $p_{\text{out}} = 0.2$. The delay δ_{ij} between a pair of neurons i and j, represents the time it takes an action potential to travel through the axon from the presynaptic neuron i to the postsynaptic neuron j, and was taken from the following distributions: For a pair of neurons belonging to the same node the delay time was derived from a uniform distribution in the range [1.5, 2.5] ms, whereas for neurons belonging to different nodes the delay was drawn from a uniform distribution in the range $[\tau - 0.5,\ \tau + 0.5]$ ms, where τ (the average time delay between two nodes) was a tuneable parameter that varied in the simulations. Reciprocal delays between two nodes were taken from the same uniform distribution with the same average delay τ.

For every neuron i in the network, the membrane potential V^i is described by the following differential equation:

$$C_m \frac{dV^i}{dt} = -g_{Na} {m^i}^3 h^i (V^i - E_{Na}) - g_k {n^i}^4 (V^i - E_k) - g_L (V^i - E_L) + I^i_{\text{syn}} + I^i_{\text{ext}} + I^i_{\text{noise}}, \quad (1)$$

where $C_m = 1\ \mu\text{F/cm}^2$ is the membrane capacitance. The constants $g_{Na} = 120\ \text{mS/cm}^2$, $g_k = 36\ \text{mS/cm}^2$ and $g_L = 0.3\ \text{mS/cm}^2$ are the maximal conductance of their corresponding channels, and $E_{Na} = 115$ mV, $E_k = -12$ mV, and $E_L = 10.5$ mV are the corresponding reversal potentials. The voltage-gated ion channels m, n, and h represent activation and inactivation of the sodium and potassium channels and can be described by the following three differential equations:

$$\frac{dX^i}{dt} = \alpha_X(V^i)(1 - X^i) - \beta_X(V^i) X^i, \quad (2)$$

where $X \equiv m,n,h$. The experimentally fitted voltage-dependent transition rates are

$$\begin{aligned} \alpha_m(V) &= \frac{0.1(V - 25)}{1 - \exp(-0.1(V - 25))} \\ \beta_m(V) &= 4\exp(-V/18) \\ \alpha_n(V) &= \frac{0.01(V - 10)}{1 - \exp(-0.1(V - 10))} \\ \beta_n(V) &= 0.125\exp(-V/80) \\ \alpha_h(V) &= 0.07\exp(-V/20) \\ \beta_h(V) &= \frac{1}{1 + \exp(-0.1(V - 30))}. \end{aligned} \quad (3)$$

In the absence of any type of noise or synaptic influence on the neuron, the steady state $V^i_{\text{rest}} = 0$ is stable. The synaptic transmission between neurons is modeled by a postsynaptic conductance change with the form of

$$\phi(t) = \exp(-t/\tau_d) - \exp(-t/\tau_r), \quad (4)$$

where the parameters $\tau_d = 10$ ms and $\tau_r = 1$ ms stand for the decay and rise time of the function and determine the duration of the response. The synaptic current $I^i_{\text{syn}}(t)$ takes the form

$$I^i_{\text{syn}} = -g_{\max} \sum_j \sum_{t_j^{sp}} \phi\left(t - t_j^{sp} - \delta_{ij}\right)(V^i - E_{\text{syn}}). \quad (5)$$

Here, j is the group of neurons coupled to neuron i. The internal sum is taken over the train of presynaptic spikes occurring at t_j^{sp} of a neuron j in the group. Excitatory and inhibitory transmissions were differentiated by setting the synaptic reversal potential to be $E_{\text{syn}} = 60$ mV or $E_{\text{syn}} = -20$ mV, respectively.

$g_{\max}$ describes the maximal synaptic conductance between neurons. In order to keep the synaptic current from growing proportionally with N, we demand that the average connectivity strength of each neuron remains constant, $p_{\text{out}} N g_{\max} = \text{const}$, where the constant value was set to 1. The conductance $g_{\max}$ for each neuron was selected randomly from the following uniform distribution $[g_{\max} - 2 \times 10^{-3}\ \text{mS/cm}^2,\ g_{\max} + 2 \times 10^{-3}\ \text{mS/cm}^2]$ in order to allow diversity of synaptic properties that might resemble actual brain connectivity.

The external stimulation current, I^i_{ext}, was set to zero for the entire network. To stimulate nodes we used an external stimulation current of 4 $\mu\text{A/cm}^2$ for 5 ms. Background noise was added as a synaptic current input from a balance network composed of 800 excitatory neurons firing randomly at about 1–3 Hz and 200 inhibitory neurons firing randomly at about 50–100 Hz. Following Eq. (5) the noise current $I^i_{\text{noise}}(t)$ takes the form

$$I^i_{\text{noise}}(t) = -\left\{ g_{\text{ex}} \sum_{k=1}^{800} \sum_{t_k^{sp}} \phi\left(t - t_k^{sp}\right)(V^i - 60) + g_{\text{in}} \sum_{k=1}^{200} \sum_{t_k^{sp}} \phi\left(t - t_k^{sp}\right)[V^i - (-20)] \right\}. \quad (6)$$

The excitatory and inhibitory synaptic conductance, g_{ex} and g_{in}, were adjusted such that a neuron that is only driven by the noise fired randomly about five spikes per second. The intercell activity fluctuates around the resting potential with a standard deviation of 5 mV, corresponding to the term silent regime demonstrated by Luccioli *et al.* [14] where the irregular activity resembles the activity of cortical neurons characterized by an almost Poissonian distribution of interspike intervals [12,21].

Quantitative measures of firing rates and relative phases were carried on simplified nodes for which inhibitory connections and background noise were omitted [Fig. 1(a) (right)]. However, the connectivity among nodes remains sparse as well as the distribution of time delays and conductance.

The set of differential equations was preliminarily solved numerically using three algorithms: the Euler method, Heun's method, and fourth-order Runge-Kutta (4RK) method, each with a time step of 0.02 ms. Results obtained by the Heun and 4RK methods were almost identical and were slightly different from attained results by the Euler method. As the complexity of the 4RK is higher the method is much more complicated to implement and is not well defined in the case of delayed equations, therefore the presented results in this paper were derived using Heun's method.

Synchronization within a given population and between populations was measured by comparing exact firing timing of individual neurons as well as firing rates. Exact firing timing was analyzed by computing a histogram of the number of neurons in a node that fire simultaneously every time step (resolution of 0.02 ms). Firing rates were determined by

a measure of the average interspike interval (ISI) of each neuron. We found that synchronization of populations was robust to the distribution of the delays and conductance. Moreover, synchronization was improved as N increased. The intuitive explanation is based on signal-to-noise ratio where every spike train of every neuron is composed of APs (spikes) and small fluctuations around the resting potential. Thus, the scaled summation of the synaptic input Eq. (5) decreases as $\frac{1}{N}$ following the central limit theorem and the signal-to-noise ratio is enhanced.

The generality of the HH simulations results was tested with a simple leaky integrate and fire (IAF) model [22] that can be described by the following equations:

$$\begin{aligned} \tau_m \dot{V}_{\text{mem}} &= -[V_{\text{mem}}(t) - V_{\text{rest}}] + RI(t) \\ RI(t) &= \tau_m A \sum_j \sum_{t_j^{sp}} \delta\left(t - t_j^{sp} - \tau\right) + \xi(t), \end{aligned} \tag{7}$$

where $\tau_m = 50$ sec is the membrane time constant. Each neuron is initialled to the rest potential of $V_{\text{rest}} = -70$ mV. Every time step (0.1 ms) the synaptic currents are summed up with an amplitude $A = 250$, and increase the membrane potential until it reached a threshold of $V_{\text{thr}} = -50$ mV, at which the neuron fires and its potential relaxes to V_{rest}. The delay between neurons from different populations, τ, was set to 40 ms. There were no connections between neurons belonging to the same population. Background noise $\xi(t)$ was added from a uniform distribution between 0–150 mV.

The activity mode of triangle motifs and chain motifs were studied as they have been found among other motifs in real neural networks such as in C. elegans [5,6]. In addition, applying the procedure of finding motifs in a graph, described in [5,6], over the cortico-cortical connections of the cat cerebral cortex [23] resulted these motifs as well.

III. ACTIVITY MODES OF MOTIFS AND SMALL NETWORKS

A. Activity modes of two nodes

The prototypical network consisting of two simplified reciprocally connected nodes via excitatory connections is depicted in Fig. 1(a). Each node consists of $N = 60$ neurons.

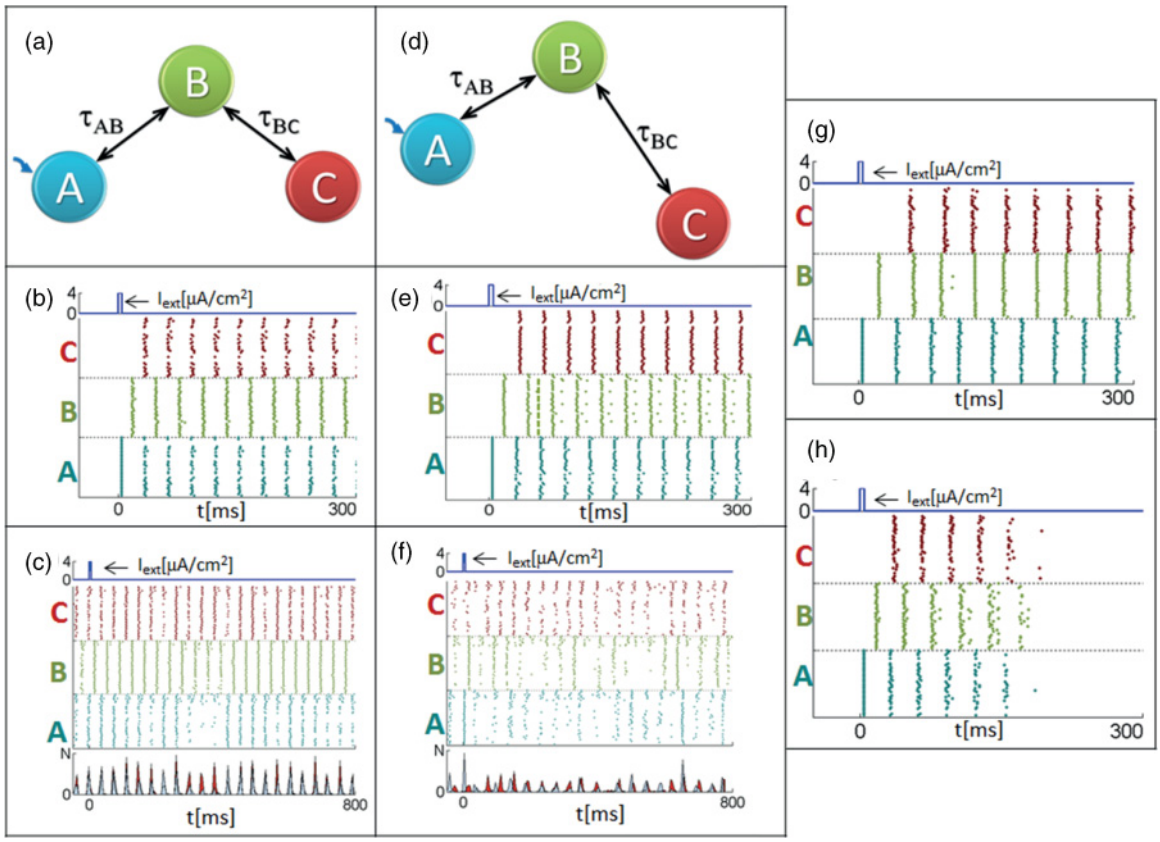

FIG. 2. (Color online) (a) Schematic diagram of a chain of three mutually connected nodes $\tau_{AB} = \tau_{BC} = 10$ ms. (b) Raster diagram of the corresponding chain, $g_{\max} = 1.08$ mS/cm^2. Variability in the spike trains of different neurons is a result of the sparse connectivity and varied delays. (c) Raster diagram of a symmetric chain where the background noise and inhibitory connections are taken into account, $\tau_{AB} = \tau_{BC} = 15$ ms. Lower panel: histogram of spike timings of nodes A (light blue) and C (dark red). (d) Schematic diagram of a chain of three mutually coupled nodes $\tau_{AB} = 10$ ms, $\tau_{BC} = 14$ ms. (e) Raster diagram of the corresponding chain with $g_{\max} = 1.8$ mS/cm^2. The dashed green line indicates the timing of an AP that should have been generated after being triggered by the AP of C. However, due to the refractory period following the previous AP of B it was suppressed. (f) Raster diagram of an asymmetric chain where the background noise and inhibitory connections are taken into account, $\tau_{AB} = 10$ ms, $\tau_{BC} = 14$ ms. Lower panel: histogram of spike timings of node A of nodes A (light blue) and C (dark Red). (g) Raster diagram of a chain with $\tau_{AB} = 15$ ms and $\tau_{BC} = 30$ ms and $g_{\max} = 1.8$ mS/cm^2. (h) sparse connectivity leads to decay in firing rates. Here $\tau_{AB} = 10$ ms and $\tau_{BC} = 14$ ms and $g_{\max} = 1.44$ mS/cm^2. Simulations parameters are: $N = 40$, $I_{\text{ext}} = 4$ μA/cm^2.

At $t = 0$ node A (blue) is stimulated for 5 ms by an external current, $I_{\text{ext}} = 4\ \mu\text{A/cm}^2$. If the short stimulation triggers enough APs in the population of neurons belonging to node A, this triggers APs in the associated node B and vice versa, and after a short transient of a few τ, the system settles into a periodic firing state in which neurons in each node tend to fire together [24,25] as depicted in Fig. 1(b). The average firing period time, T, was defined by the average ISI over time and neurons. Simulations indicated that the period time T depends linearly on the sum of the average time it takes an AP to travel through the axon of a neuron in A and through the synapse of a neuron in B, τ_{AB}, and h—the time it takes to produce an AP. h was measured in the simulation to be a few ms. Thus, an AP in A triggers an AP in B after an average delay of $\tau_{AB} + h$ and vice versa. If the returning AP arrives after the refractory period, A and B will fire periodically with a time period T that is simply the time it takes an action potential in A to travel to B and return to A [Fig. 1(c)]. Although the firing rate of the two nodes is identical, they do not fire simultaneously but are shifted with a constant phase of $T/2$ ms denoted as antiphase synchronization [15]. Similar results were obtained when the background noise and the inhibitory connections were taken into account [Fig. 1(d)]. A histogram of spike timings of neurons in node A is presented at the bottom panel of Fig. 1(d) indicating the low rate and irregular nature of the simulated firing. A closer examination of several neurons in node A [Fig. 1(e)] reveals that the firing pattern of every individual neuron is very different. In fact, the oscillatory nature is only noticeable when looking at the firing patterns of entire populations, similar to what we would expect to find in experimental findings [12].

B. Activity modes of motifs of size three

Three nodes that are coupled reciprocally can form either a chain motif or a triangle motif. The firing dynamics of a chain motif can be derived from the case of two nodes. Every node is in antiphase synchronization (constant phase of $T/2$ ms) with respect to its neighbors. Consequently, a subchain structure emerges, in which the chain is divided into two synchronized groups, odd and even nodes [26]. Each group is synchronized in zero lag and the delay between the groups is $T/2$ ms. Figure 2(a) depicts the case of a chain of three nodes, where A and C are synchronized in zero lag and B is shifted with time delay $T/2$ ms [Fig. 2(b)]. Similar results were obtained when the inhibitory connections and the noise were taken into account as depicted in Fig. 2(c). However, a nonsymmetric chain of three nodes with two different delay times, $\tau_{AB} < \tau_{BC}$ [Fig. 2(d)] exhibits the following two main types of activities, which depend on the refractory period, t_{ref} that was measured in simulation to be around 7 ms: (i) $2(\tau_{BC} - \tau_{AB}) \leqslant t_{\text{ref}}$ [and Figs. 2(e) and 2(f)], the middle node B is not able to fire in response to C, since the response time falls within the refractory period. The resulting averaged

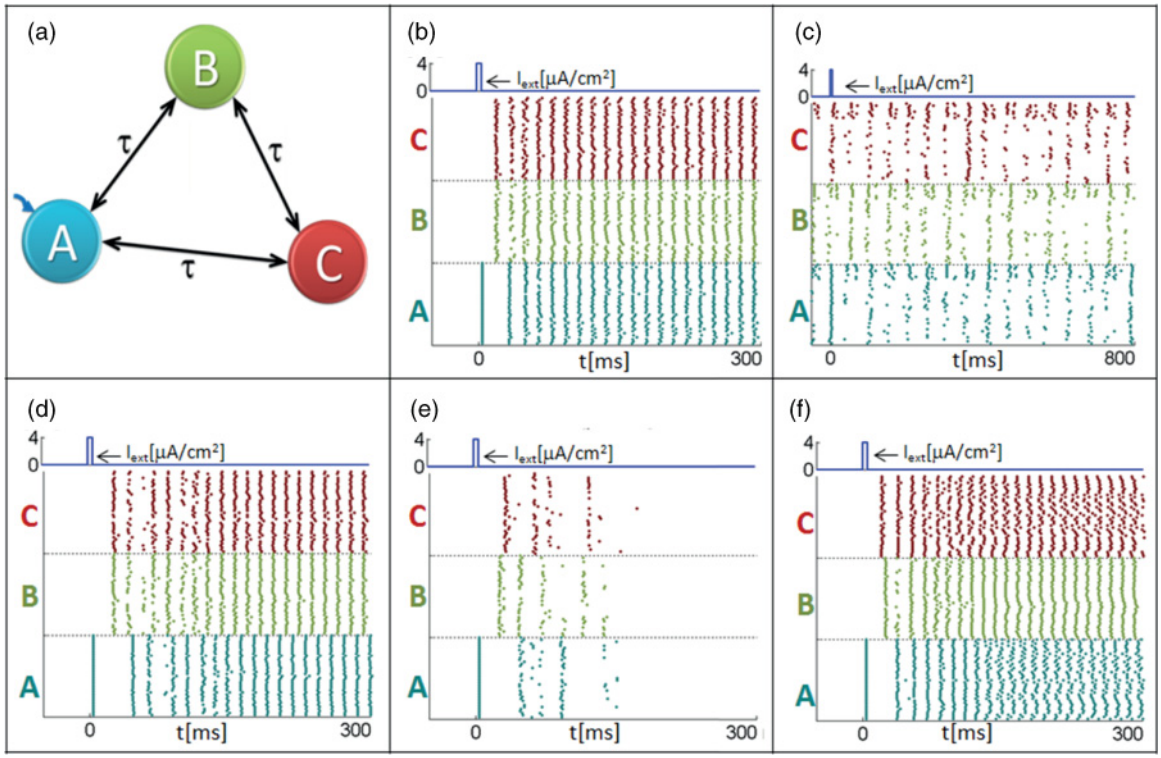

FIG. 3. (Color online) (a) Schematic diagram of a triangle $\tau_{AB} = \tau_{BC} = \tau_{AC} = \tau = 10$ ms, $g_{\max} = 1.8$ mS/cm^2. (b) Raster diagram of the triangle. (c) Raster diagram of the triangle,where the background noise and inhibitory connections are taken into account. $g_{\max} = 1.44$ mS/cm^2. (d) Raster diagram of an isosceles triangle, $\tau_{AB} = \tau_{AC} = 17$ ms, $\tau_{BC} = 10$ ms, $g_{\max} = 0.72$ mS/cm^2. B and C are in ZLS and A is shifted with a constant delay. (e) Raster diagram of a triangle, $\tau_{AB} = 17$ ms, $\tau_{AC} = 23$ ms, $\tau_{BC} = 10$ ms, $g_{\max} = 0.72$ mS/cm^2. Since no mode is stable the firing terminates. (f) Raster diagram of the same triangle as in (e), but with $g_{\max} = 1.44$ mS/cm^2. By increasing the synaptic strength it is possible to reach a stable firing mode. Simulations parameters are: $N = 40$, $I_{\text{ext}} = 4\ \mu\text{A/cm}^2$.

ISI is $2\tau_{AB} + 2h$ and is identical for the three nodes, A and B are in the antiphase state and C is shifted with some constant phase different from $T/2$. (ii) $2(\tau_{BC} - \tau_{AB}) > t_{\text{ref}}$ [Fig. 2(g)], an AP from C does not fall within the refractory period and B responds to both A and C, which results in alternating periods. Note that when the synaptic strength is weak, reverberation will diminish and firing of all nodes will be terminated in a short time [Fig. 2(h)].

An equilateral triangle [Fig. 3(a)] ($\tau_{AB} = \tau_{AC} = \tau_{BC} = \tau$) exhibits ZLS with an average ISI equal to $\tau + h$ ms for τ larger than the refractory period ($\tau > t_{\text{ref}}$), as exemplified in Figs. 3(b) and 3(c) for the case of additional background noise and inhibitory connections. However, other triangles exhibit symmetry breaking among the ZLS activity of the three nodes depending on the specific delay times. For example, an isosceles triangle can exhibit ZLS between nodes B and C while node A is shifted [Fig. 3(d)]. In a triangle with three different delays the firing of all nodes may be terminated because there is no stable firing mode [Fig. 3(e)]; however, when the synaptic strength is increased a stable firing state in which every node is shifted from the others with a constant delay is achieved [Fig. 3(f)].

Our results indicate that the same topology but with different network parameters results in a manifold of different activities, suggesting that the dynamic behavior of neural networks is too complex to be described solely by topological motifs. Each motif actually represents a family of comprehensive motifs that differ from one another by their network parameters, resulting in diverse activity modes, which ultimately enrich the network functionality. This calls for reevaluating the importance of motifs that appear significantly more than expected in random networks.

C. Activity modes of small networks

We now turn to discuss the case of small networks constructed from several motifs, where every motif has more than one possible activity mode depending on the network parameters. Do the connected motifs maintain their characteristic behavior? Or does one motif take over the whole activity mode of the network? Simulations indicate that local changes in topology affect even remote nodes in the network. Consider the network in Figs. 4(a)–4(c) consisting of two motifs, a chain and a triangle, where each motif is responsible for a different behavior; a firing period of $\tau + h$ for the triangle and of $2(\tau + h)$ for the chain. The shorter period, (faster frequency), takes over and the whole network fires with zero lag and with period $\tau + h$. When the connection between D and E is removed [Figs. 4(d)–4(f)], the new topology of the network consists of two overlapping chains of four nodes, where the additional node E is a replica of D by receiving the same drive. Nodes A and C are synchronized in zero lag, and B, D, and E are also synchronized in zero lag and the two groups are in antiphase with each other. When the background noise and inhibitory connections were taken into account, we found that while the firing patterns were less ordered, the main

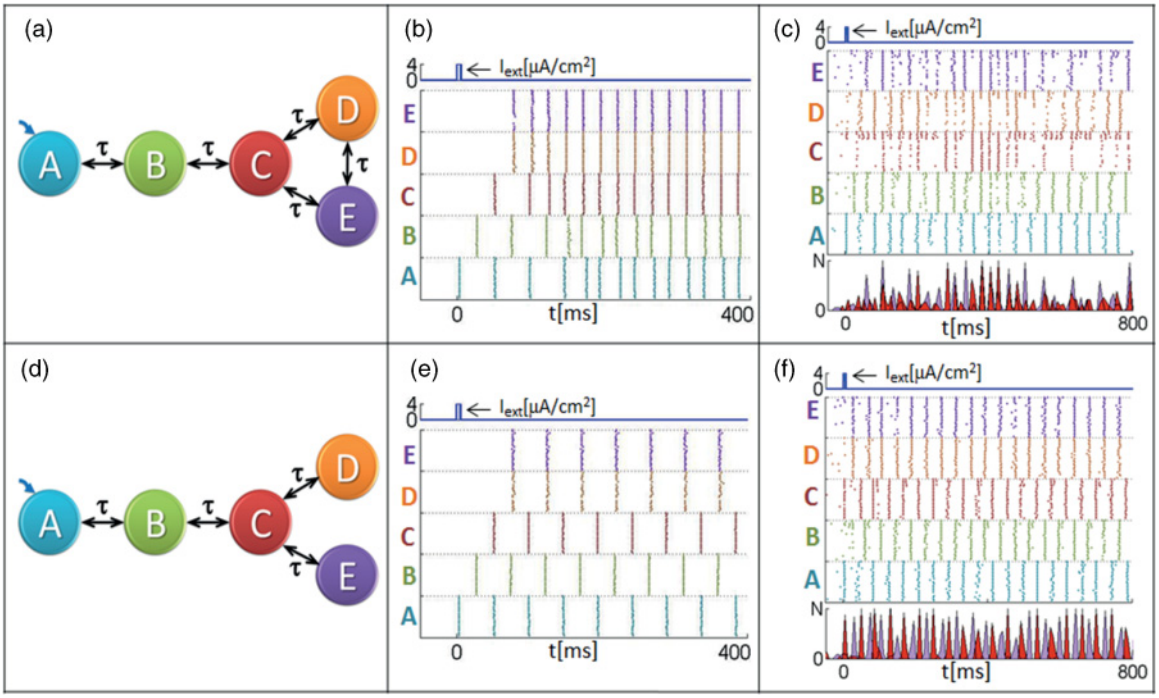

FIG. 4. (Color online) (a) Schematic diagram of a small network. (b) Raster diagram of the network in (a), $g_{\max} = 1.44$ mS/cm^2 and $\tau = 15$ ms. (c) Raster diagram of the network in (a) where the background noise and inhibitory connections are taken into account. Lower panel: histogram of spike timings of node C (dark red) and E (light violet). $g_{\max} = 1.08$ mS/cm^2 and $\tau = 10$ ms. (d) Schematic diagram of a small neural network similar to (a) where the bidirectional connection between D and E is removed. (e) Raster diagram of the network in (d), $g_{\max} = 1.44$ mS/cm^2 and $\tau = 15$ ms. (f) Raster diagram of the network in (d) where the background noise and inhibitory connections are taken into account. Lower panel: histogram of spike timings of node C (dark red) and E (light violet). $g_{\max} = 1.08$ mS/cm^2 and $\tau = 10$ ms. Simulations parameters are: $N = 24$, $I_{\text{ext}} = 4\ \mu$A/cm^2.

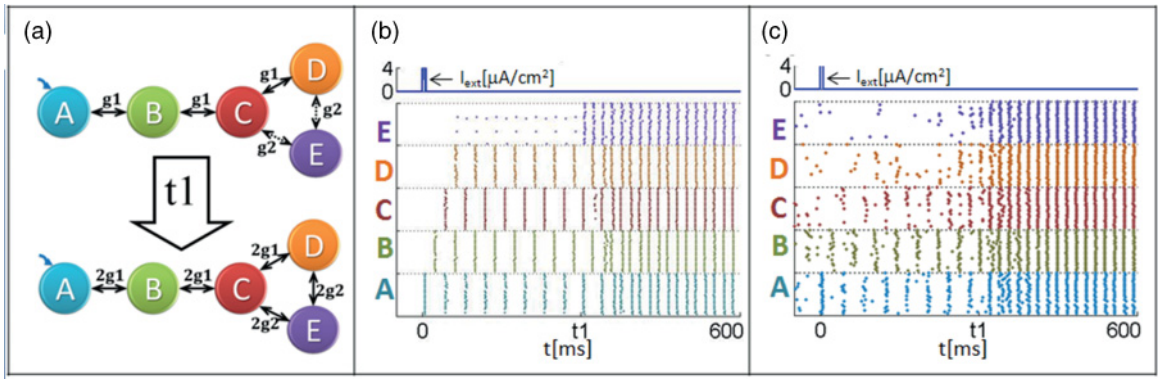

FIG. 5. (Color online) (a) An example of how a change in a synaptic strength changes the activity mode of the network. In the small network, the connections to and from E are weak, whereas the connections between other nodes are strong. By increasing the synaptic strength to and from node E, E becomes synchronized with A, B, C, and D. (b) Raster diagram of the network with $g1 = 1.44$ mS/cm^2. At $t1 = 300$ ms. The synaptic connections were enhanced by doubling $g1$ and $g2$. (c) Raster diagram of the network where the background noise and inhibitory connections are taken into account, with $g1 = 1.8$ mS/cm^2. Simulations parameters: $N = 40$, $g2 = g1/3$, $I_{\text{ext}} = 4\ \mu$A/cm^2, $\tau = 15$ ms.

results remain valid as depicted in Figs. 4(c) and 4(f). This example illustrates that by eliminating the local connection between D and E the activity mode of the entire network is changed.

Modes of activity of a network can be time dependent as a function of the dynamic re-scaling of synaptic strengths. Consider the network in Fig. 5(a), The four nodes A, B, C, D form a chain. The bidirectional connections with node E form a triangle, however they are very weak in comparison with the other connections. The firing rate of the network is $2(\tau + h)$ and the nodes synchronized alternately: nodes A and C are in ZLS, nodes B and D are in ZLS as well, but in an antiphase (shift of $T/2$ ms) with respect to A and C, and node E is not firing at all. At $t = t1$ the synaptic connections are strengthened [imitating learning processes such as long-term plasticity (LTP)]. Node E starts reverberating with C and D and forms a triangle motif with a doubled firing rate, which ultimately takes over the entire network resulting ZLS of all nodes [Figs. 5(b) and 5(c)]. Thus, long-term synaptic plasticity may permanently affect the nature of the stable modes of activity in the network without altering either the topology of the network or the time delays, but so do changes in synaptic activity brought about by neuromodulators for shorter periods. Even changes in synaptic efficiency, which depend on short-term past activity in a given node [27,28] may determine the overall activity of the entire network. This example demonstrates that a change in the synaptic strength can modify the firing rate and lead to different synchronization modes in which correlations between the activity of remote nodes are altered.

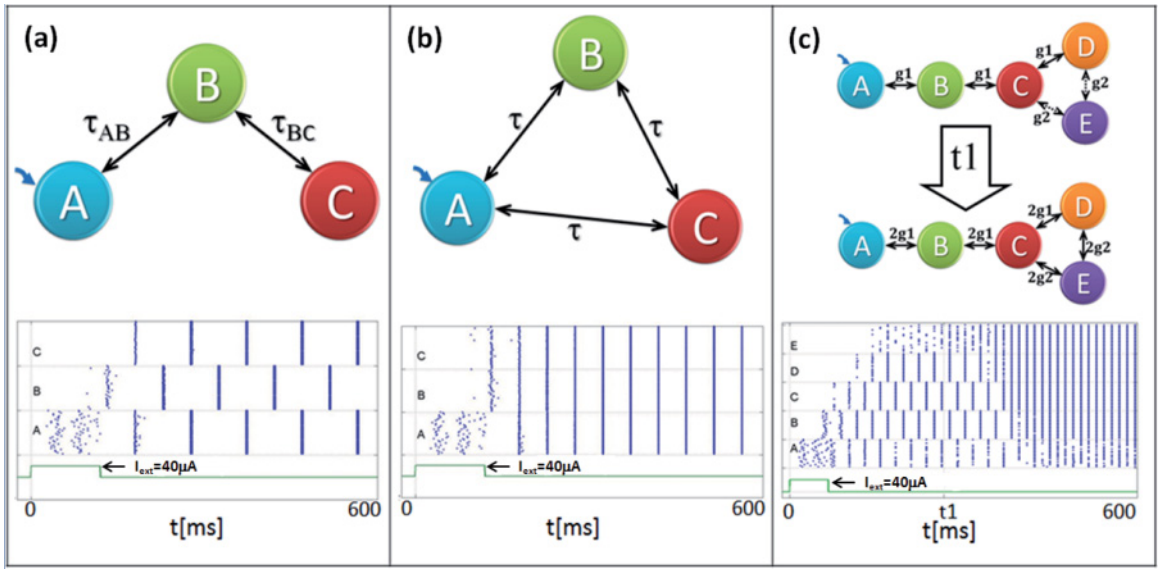

FIG. 6. (Color online) Schematic diagrams and raster diagrams obtained for different networks with a simple leaky integrate and fire (IAF) model replacing the HH model for every neuron. (a) Results for the chain motif $\tau_{AB} = \tau_{BC} = 40$ ms. (b) Results for the triangle motif $\tau = 40$ ms. (c) results for a dynamical process described in Fig. 4, $\tau = 40$ ms. Here, the conductance $g1$ are modeled by the amplitude of $A = 250$ and $g2$ as an amplitude of $A = 80$.

Results with a simple leaky integrate and fire (IAF) model replacing the HH model for every neuron obtained for the chain motif, the triangle motif, and a small network are presented in Fig. 6, indicating that our general conjecture is independent of the HH characteristics.

IV. CONCLUSION

Our findings suggest that the appearance of significant topological motifs in a neural network is not sufficient to determine the network's modes of activity. Rather, the motif parameters (i.e., the delays, the neuronal properties, and the synaptic strength), which together with the topology form a comprehensive motif may better capture the network's capabilities and functionality. For example, enhancing synaptic strength of one or more nodes may result in different stable modes of reverberations. Thus, the reverberation modes may hold a temporary memory of the nature of the initiating stimulus both in the spatial domain (which node was stimulated) and in the temporal domain (the time relations between the initial activation of some of the nodes). Therefore, a comprehensive motif that enriches the functionality of neural networks by exhibiting diverse operation modes with similar topology should become a fundamental concept in neural network research.

For larger networks with a variety of delay times and for external stimuli it is expected that the number of possible modes of activity will increase; however, the scaling relation between the number of activity modes as a function of the size of the network is currently an open question. Sensitivity to local changes in the network parameters was observed for both chains and networks with feedback loops, but is expected to disappear for fully connected networks in which a mean-field-like behavior arises where dynamics is insensitive to the details of the network parameters. For example, van Vreeswijk *et al*. [20,29] demonstrate that balanced networks of inhibitory and excitatory neurons with sparse local random connections have a chaotic attractor, which is insensitive to many details of the neurons and network connectivity. This result further reinforces our findings, which question the relevance of motifs to the global neural network dynamical properties. An interesting open question is how to classify additional modes of activity that can be achieved only with networks consisting of feedback loops.

In this study we focus on synchronized modes of oscillatory neurons. Our results are also supported by recent experimental recording of irregular firing neurons revealing that it is unlikely that local motifs can explain global structure. For example, the pyloric network of the stomatogastric ganglion (STG) of P. interruptus is one of the best understood pattern-generating circuits. The connectivity among these neurons and their intrinsic membrane properties have been determined [30–33]. Nevertheless, experimental studies [34–39] have established that this fixed 30-neuron network can switch between many different dynamic modes. Another example is the C. elegans nervous system that can produce different dynamics by adjusting the level of a neuromodulator [40]. These two examples demonstrate that a network with fixed topology can result in different dynamic modes regardless of their fixed motif structure.

Each node in our model consisted of a few tens of neurons, whereas in reality there are several thousands. Increasing the number of neurons in each node in our model should improve the signal-to-noise ratio, as discussed in the methods section, and in fact allows for a larger variability in the network parameters and thus improves the network's stability. In our model, connections within each node were limited to excitatory-inhibitory connections and vice versa. Preliminary results confirm the robustness of our results to additional weak self-excitation and inhibition within each node. We also expect results to be robust for other variations in neuronal properties as the number of neurons within each node increases. An extreme case would be a cortical patch containing several subgroups each with a unique receptive field or sensory properties, such as the orientation selective neurons in a hypercolumn of the primary visual cortex. In this case, it is likely that each subgroup would be best treated as an independent patch. This calls for future studies as well as a quantitative comparison through experimental research such as artificial construction of small motifs on cultured neurons.

[1] S. H. Strogatz, Nature (London) **410**, 268 (2001).
[2] M. Newman, SIAM Rev. **45**, 167 (2003).
[3] A. L. Barabasi and R. Albert, Science **286**, 509 (1999).
[4] D. J. Watts and S. H. Strogatz, Nature (London) **393**, 440 (1998).
[5] R. Milo, S. Shen-Orr, S. Itzkovitz, N. Kashtan, D. Chklovskii, and U. Alon, Science **298**, 824 (2002).
[6] R. Milo, S. Itzkovitz, N. Kashtan, R. Levitt, S. Shen-Orr, I. Ayzenshtat, M. Sheffer, and U. Alon, Science **303**, 1538 (2004).
[7] O. Sporns and R. Kotter, Plos Biol. **2**, 0020369 (2004).
[8] A. R. McIntosh, M. N. Rajah, and N. J. Lobaugh, Science **284**, 1531 (1999).
[9] M. Steriade, D. A. McCormick, and T. J. Sejnowski, Science **262**, 679 (1993).
[10] R. Eckhorn, R. Bauer, W. Jordan, M. Brosch, W. Kruse, M. Munk, and H. J. Reitboeck, Biol. Cybern. **60**, 121 (1988).
[11] C. M. Gray, P. Konig, A. K. Engel, and W. Singer, Nature (London) **338**, 334 (1989).
[12] M. Abeles, *Corticonics: Neural Circuits of the Cerebral Cortex* (Cambridge University Press, Cambridge, 1991).
[13] S. Strogatz, *Nonlinear Dynamics and Chaos* (Westview Press, Boulder, 1994).
[14] S. Luccioli, T. Kreuz, and A. Torcini, Phys. Rev. E **73**, 041902 (2006).
[15] M. H. Park and S. Kim, J. Korean Phys. Soc. **29**, 9 (1996).
[16] A. L. Hodgkin and A. F. Huxley, J. Physiol. **117**, 500 (1952).
[17] V. Braitenberg and A. Shuz, *Cortex: Statistics and Geometry of Neural Connectivity* (Springer, Berlin, 1998).
[18] E. V. Evarts, J. Neurophysiol. **27**, 152 (1964).

[19] N. Brunel, J. Comput. Neurosci. **8**, 183 (2000).
[20] C. A. van Vreeswijk and H. Sompolinsky, Science **274**, 1724 (1996).
[21] M. N. Shadlen and W. T. Newsome, J. Neurosci. **18**, 3870 (1998).
[22] C. Koch and I. Segev, *Methods in Neuronal Modeling* (MIT Press, Cambridge, MA, 1998).
[23] J. W. Scannell, C. Blakemore, and M. P. Young, J. Neurosci. **15**, 1463 (1995).
[24] J. M. Casado and J. P. Baltanas, Phys. Rev. E **68**, 061917 (2003).
[25] M. Diesmann, M. O. Gewaltig, and A. Aertsen, Nature (London) **402**, 529 (1999).
[26] J. Kestler, W. Kinzel, and I. Kanter, Phys. Rev. E **76**, 035202 (2007).
[27] A. M. Thomson and J. Deuchars, Trends Neurosci. **17**, 119 (1994).
[28] M. V. Tsodyks and H. Markram, Proc. Natl. Acad. Sci. USA **94**, 719 (1997).
[29] C. A. van Vreeswijk and H. Sompolinsky, Neural Comput. **10**, 1321 (1998).
[30] A. I. Selverston and J. P. Miller, J. Neurophysiol. **44**, 1102 (1980).
[31] J. S. Eisen and E. Marder, J. Neurophysiol. **48**, 1392 (1982).
[32] J. P. Miller and A. I. Selverston, J. Neurophysiol. **48**, 1378 (1982a).
[33] J. P. Miller and A. I. Selverston, J. Neurophysiol. **48**, 1416 (1982b).
[34] J. L. Ayers and A. I. Selverston, J. Comput. Phys. A **129**, 5 (1979).
[35] E. Rezer and M. Moulins, J. Comput. Phys. A **153**, 17 (1983).
[36] J. S. Eisen and E. Marder, J. Neurophysiol. **51**, 1375 (1984).
[37] G. G. Turrigiano and H. G. Heinzel, Cambridge (1992).
[38] S. L. Hooper, J. Comput. Neurosci. **4**, 191 (1997a)
[39] S. L. Hooper, J. Comput. Neurosci. **4**, 207 (1997b)
[40] M. Tsunozaki, S. H. Chalasani, and C. I. Bargmann, Neuron **59**, 959 (2008).